Robotica (2016) volume 34, pp. 449–467. © Cambridge University Press 2014
doi:10.1017/S0263574714001581

Adaptive dynamic surface control for vision-based stabilization of an uncertain electrically driven nonholonomic mobile robot

Zhengcai Cao†,‡*, Longjie Yin†,‡, Yili Fu‡ and Jian S Dai§

†*College of Information Science and Technology, Beijing University of Chemical Technology, Beijing 100029, China*
‡*State Key Laboratory of Robotics and System, Harbin Institute of Technology, Harbin 150080, China*
§*Centre for Robotics Research, King's College London, London WC2R 2LS, UK*

(Accepted May 27, 2014. First published online: July 10, 2014)

SUMMARY
This paper investigates the vision-based pose stabilization of an electrically driven nonholonomic mobile robot with parametric uncertainties in robot kinematics, robot dynamics, and actuator dynamics. A robust adaptive visual stabilizing controller is proposed with the utilization of adaptive control, backstepping, and dynamic surface control techniques. For the controller design, the idea of backstepping is used and the adaptive control approach is adopted to deal with all uncertainties. We also apply the dynamic surface control method to avoid the repeated differentiations of virtual controllers existing in the backstepping design procedure such that the control development is easier to be implemented. Moreover, to attenuate the effect of disturbances on control performance, smooth robust compensators are exploited. It is proved that all signals in the closed-loop system can be guaranteed to be uniformly ultimately bounded. Finally, simulation results are presented to illustrate the performance of the proposed controller.

KEYWORDS: Actuator dynamics; Adaptive control; Dynamic surface control; Vision-based stabilization; Nonholonomic mobile robot.

1. Introduction

During the past few years, the use of visual information in the feedback loop for motion control of nonholonomic mobile robots (NMR) has received wide attention and is a topic of great research interest. Many studies have been carried in this field and can be divided into two main portions: visual tracking and visual stabilization. Here we consider the problem of vision-based stabilization of a nonholonomic mobile robot with an onboard monocular vision system. The basic idea is using visual feedback to drive robot from an initial pose to the desired one, which is specified by an image previously taken at the target pose.

For the vision-based stabilization of NMR, much work has been done. A traditional approach is to perform motion based on the epipolar geometry.[1–3] However, the epipolar geometry becomes ill-conditioned for planar scenes, which are quite common in human environments. A good alternative is the homography-based approach,[4,5] but the homography model is not well defined if there is no dominant plane in the scene or with large baselines. In ref. [6], a switching control scheme based on the epipolar geometry and homography was proposed, which took advantage of both models avoiding the drawbacks of each one and allowing a smooth motion of robot. Another feasible way to overcome the drawbacks of these two geometric constraints is to use trifocal tensor,[7,8] which

* Corresponding author. E-mail: giftczc@163.com

describes the relative geometry of three views completely and is independent of the observed scene. Recently, Zhang *et al*.[9] proposed a hybrid vision-based stabilization strategy based on a motion-estimation technique, which can be applied in both planar and non-planar scenes and required no matrix estimation or decomposition. In ref. [10], two-phase technique was used to present a robust controller that enabled the mobile robot pose regulation in spite of lack of both depth information and precise visual parameters. The above-mentioned methods, however, are based on robot kinematics only and the nonlinear forces in robot dynamics are neglected. There have been few researches where the dynamics of mobile robot is considered to achieve the vision-based stabilization. In ref. [11], a feedback dynamic control law based on backstepping technique was presented for a wheeled mobile robot to perform position-based visual servo stabilization. In ref. [12], considering uncertainties in robot dynamics, an adaptive sliding-mode dynamic stabilizing controller was proposed.

In summary, the aforementioned approaches are of important reference in vision-based pose stabilization of NMR. However, the proposed controllers in these schemes are designed at kinematic level with velocity as input, or at dynamic level with torque as input without considering the actuator dynamics. As demonstrated in ref. [13], the actuator dynamics is an important part of complete robot dynamics, especially in the case of highly varying loads and high-velocity movement. In practice, as the wheels of the robot are driven by actuators, it is more realistic to formulate the motion control problem of NMR at actuator level, where the actuator voltages are taken as control inputs. Many control strategies have therefore been developed for mobile robots incorporating actuator dynamics.[14–16] Unfortunately, these developments are devoted to the tracking control of NMR and cannot be applied directly to stabilization problem due to restrictions on reference velocity (i.e., the reference linear velocity does not converge to zero), and it is assumed that full robot states are available, which is clearly not true for the monocular vision system because of unknown depth information. Moreover, most of the proposed controllers for the vision-based pose stabilization of NMR in the literature do not consider uncertainties in robot kinematics.

Accordingly, this paper addresses the vision-based pose stabilization problem of a nonholonomic mobile robot incorporating actuator dynamics with uncertainties and external disturbances. All parameters of robot kinematics, robot dynamics, and actuator dynamics are assumed to be unknown. As the presence of actuator dynamics increases the complexity of system dynamics, and when the mobile robot includes uncertainties of robot kinematics and dynamics as well as uncertainties of actuator dynamics, the controller design problem becomes extremely difficult. To solve this stabilization problem, a simple robust adaptive controller is developed by combining dynamic surface control (DSC) with backstepping and adaptive control inspired by the work given in refs. [14, 16]. For controller design, the idea of backstepping is used, which breaks down complex nonlinear systems into smaller subsystems such that the design procedure is systematic and simple. At the same time, by using the DSC technique, which has been much studied in ref. [17], the complexity of the controller caused by repeated derivatives of virtual controllers in the backstepping design procedure is reduced. All parametric uncertainties are treated by the adaptive technique, and smooth robust compensators are applied to counteract external disturbances. Besides, the simplified parameter estimation technique presented in ref. [14] is used to reduce the number of tuning parameters. The proposed control scheme can ensure that all signals in the closed-loop system are uniformly ultimately bounded.

This paper is organized as follows. Section 2 describes the mathematical modeling that is used for the mobile robot–camera, and the robot–camera-target. Section 3 formulates the vision-based stabilization problem. The controller design procedure and the stability analysis of the closed-loop system are detailed in Sections 4 and 5 respectively. Simulation results are presented in Section 6. Finally, Section 7 concludes the paper.

2. Mathematical Modeling

In this section, the mobile robot model, the camera model, and the robot–camera–target model are briefly introduced, which are keys to the development of our controller.

2.1. Model of a nonholonomic mobile robot

As illustrated in Fig. 1, a mobile robot with two actuated wheels is used, and a monocular camera is fixed on board. $O - XYZ$ is the reference coordinate system, $o - x_r y_r$ and $C - x_c y_c z_c$ are the coordinate systems fixed to the mobile robot and the camera respectively. The middle between

https://doi.org/10.1017/S0263574714001581 Published online by Cambridge University Press

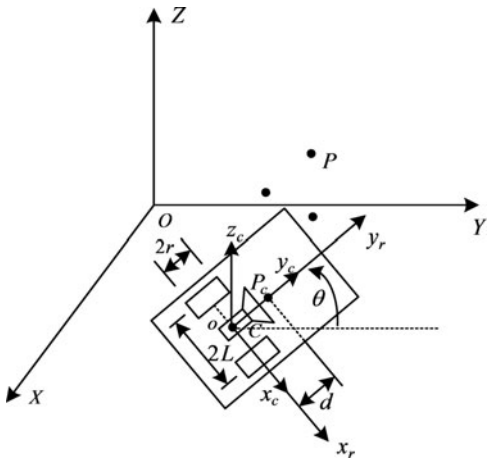

Fig. 1. Mobile robot with monocular camera.

the left and right driving wheels, o, is the origin of the coordinate system $o - x_r y_r$; C, the origin of the coordinate system $C - x_c y_c z_c$, is located at the camera center coincident with o; P_c is the mass center of the mobile robot; d is the distance from o to P_c; r is the radius of the wheel, and $2L$ is the distance between the two driving wheels. Note that the camera is placed in such a way that the robot and camera frames are aligned.

The kinematics and dynamics of nonholonomic mobile robot. including the actuator dynamics, are described by[18,16]

$$\dot{q} = J(q)w, \tag{1}$$

$$\bar{M}(q)\dot{w} + \bar{V}(q, \dot{q})w + \bar{\tau}_d = \bar{B}\tau, \tag{2}$$

$$\bar{L}_a\dot{\tau} + \bar{R}_a\tau + K_e N w + u_d = u, \tag{3}$$

where $q = (x, y, \theta)^T$; $(x, y)^T$ is the coordinate of o in the reference coordinate system, θ is the heading orientation taken counterclockwise from the OY-axis; $w = (w_1, w_2)^T$ and w_1, w_2 represent the angular velocities of right and left wheels respectively; $\bar{\tau}_d = (\bar{\tau}_{d1}, \bar{\tau}_{d2})^T$ and $u_d = (u_{d1}, u_{d2})^T$ denote the bounded unknown disturbances; $\tau = (\tau_1, \tau_2)^T$ is the control torque applied to the right and left wheels of the robot; $u \in R^2$ is the input voltage,

$$J(q) = 0.5r\begin{pmatrix} -\sin\theta & -\sin\theta \\ \cos\theta & \cos\theta \\ L^{-1} & -L^{-1} \end{pmatrix}, \quad \bar{M} = \begin{pmatrix} m_1 & m_2 \\ m_2 & m_1 \end{pmatrix},$$

$$\bar{V} = 0.5L^{-1}r^2 m_b d\begin{pmatrix} 0 & \dot{\theta} \\ -\dot{\theta} & 0 \end{pmatrix}, \quad \bar{B} = \begin{pmatrix} 1 & 0 \\ 0 & 1 \end{pmatrix},$$

$$m_1 = 0.25L^{-2}r^2(mL^2 + I_0) + I_w,$$

$$m_2 = 0.25L^{-2}r^2(mL^2 - I_0),$$

$$m = m_b + 2m_w, \quad I_0 = m_b d^2 + 2m_w L^2 + I_c + 2I_m,$$

$$\bar{L}_a = L_a(NK_T)^{-1}, \quad \bar{R}_a = R_a(NK_T)^{-1}.$$

In these expressions, m_b and m_w are the mass of the body and wheel with a motor respectively. I_c, I_w, and I_m are the moment of inertia of the body about the vertical axis through P_c, the wheel with a motor about the wheel axis, and the wheel with a motor about the wheel diameter respectively. $L_a = \text{diag}(l_{a1}, l_{a2})$ is the electrical inductance, $R_a = \text{diag}(r_{a1}, r_{a2})$ is the resistance, $K_T = \text{diag}(k_{t1}, k_{t2})$ is the motor torque constant, $N = \text{diag}(n_1, n_2)$ is the gear ratio, and $K_e = \text{diag}(k_{e1}, k_{e2})$ is the back electromotive force coefficient.

https://doi.org/10.1017/S0263574714001581 Published online by Cambridge University Press

Assumption 1: The disturbances $\bar{\tau}_d$ and u_d are bounded such that $\|\bar{\tau}_d\| \leq d_1$, $\|u_d\| \leq d_2$ with d_i, $i = 1, 2$ positive constants.

Assumption 2: All parameters of robot kinematics (1), robot dynamics (2), and actuator dynamics (3) are constants, but unknown.

Remark 1: Assumption 1 is used to facilitate stability analysis. Since kinematic and dynamic parameters of the whole robot system are geometric and physical, such parameters can be obtained easily and are reasonably assumed to be constants in this paper. However, since measurements may be inaccurate and the wheels of the robot may be attrited, in practice, there are uncertainties in the whole robot system. Therefore, it is necessary to develop a control law that does not require the knowledge of these parameters. All parameters of robot kinematics, robot dynamics, and actuator dynamics are assumed to be unknown in the development of controller.

2.2. Camera model

The camera model shows the relationship between the target point in the 3D Euclidean space and its projective point in the image space. Consider three static feature points in the scene (Fig.1). Based on the perspective model,[2] the following relationship can be obtained:

$$\begin{cases} \mu = f k_\mu \dfrac{x_c}{y_c} + \mu_0, \\ \upsilon = f k_\upsilon \dfrac{z_c}{y_c} + \upsilon_0, \end{cases} \tag{4}$$

where $(x_c, y_c, z_c)^T$ is the 3D Euclidean coordinate of the feature point P expressed in the camera frame $C - x_c y_c z_c$, $(\mu, \upsilon)^T$ is the corresponding image pixel coordinate, f is the focal length of the camera, k_μ, k_υ are the number of pixels per unit distance in image coordinates, and $(\mu_0, \upsilon_0)^T$ is the coordinate of the principal point in pixels. We assume that the principal point is in the center of the image ($\mu_0 = 0$, $\upsilon_0 = 0$).

Let $p = (p_1, p_2)^T$ denotes the 2D image coordinate of point P. For simple geometric analysis, it is clear that

$$\begin{cases} p_1 = f \dfrac{x_c}{y_c}, \\ p_2 = f \dfrac{z_c}{y_c}. \end{cases} \tag{5}$$

Based on (4) and (5), it is obvious that the 2D image coordinate $p = (p_1, p_2)^T$, which will be further used to construct the error signal that is described in Section 3, can be calculated from the image pixel coordinate as follows:

$$\begin{pmatrix} p_1 \\ p_2 \end{pmatrix} = \begin{pmatrix} \dfrac{\mu - \mu_0}{k_\mu} \\ \dfrac{\upsilon - \upsilon_0}{k_\upsilon} \end{pmatrix}. \tag{6}$$

2.3. Robot–camera–target model

The robot–camera–target model describes the dynamic behavior of the target in the camera frame related to the robot motion. Based on the geometric analysis of coordinate systems (Fig. 1), the following relationship can be derived:

$$\begin{cases} X = x_r \cos\theta - y_r \sin\theta + x, \\ Y = x_r \sin\theta + y_r \cos\theta + y, \\ x_r = x_c, \\ y_r = y_c, \end{cases} \tag{7}$$

https://doi.org/10.1017/S0263574714001581 Published online by Cambridge University Press

where $(X, Y)^T$ and $(x_r, y_r)^T$ are the coordinates of point P with respect to the reference coordinate system and the robot coordinate system respectively. It is clear that $(X, Y)^T$ is constant.

After taking the time derivative of (7) and using (1), we can obtain the robot–camera–object model, i.e., the velocity of point P in the camera frame related to the robot motion, as follows:

$$\begin{cases} \dot{x}_c = \dfrac{r}{2L}(w_1 - w_2)y_c, \\ \dot{y}_c = -\dfrac{r}{2}(w_1 + w_2) - \dfrac{r}{2L}(w_1 - w_2)x_c. \end{cases} \tag{8}$$

3. Problem Statement

In general, the vision-based stabilization problem can be regarded as using image feedback to drive mobile robot to a desired pose such that the current image (i.e., the image taken during the navigation) and the desired image (i.e., the image taken at the desired pose previously) are the same, that is, the image coordinates of the feature point P in the current and desired images are coincident with each other.

Assumption 3: Three feature points in the scene can always be extracted from the images for the vision-based stabilization task, and there exists the image feature point P satisfying $z_c \neq 0$.

Remark 2: Assumption 3 is used to ensure that the observed target remains visible during the servoing process, and to facilitate the error signal construction. If some targets get out of the camera's field-of-view, the value of current features can no longer be computed, which leads to interruption in control algorithm, that is, the failure of servoing.

Due to the planar motion of mobile robot, the height information z_c remains constant during the navigation. Therefore, for convenience, we define the following auxiliary signal, $s \in R^2$:

$$s = (s_1, s_2)^T = \left(\frac{x_c}{z_c}, -\frac{y_c}{z_c}\right)^T. \tag{9}$$

Based on (5) and (9), it is clear that the signal s can be calculated as follows:

$$\begin{cases} s_1 = \dfrac{p_1}{p_2}, \\ s_2 = -f\dfrac{1}{p_2}. \end{cases} \tag{10}$$

Correspondingly, the signal $s^* = (s_1^*, s_2^*)^T$ at the desired pose is defined by

$$\begin{cases} s_1^* = \dfrac{p_1^*}{p_2^*}, \\ s_2^* = -f\dfrac{1}{p_2^*}, \end{cases} \tag{11}$$

where $(p_1^*, p_2^*)^T$ is the desired image coordinate of the feature point P, and can be computed through the camera model from the desired image.

Then to achieve the vision-based stabilization task and facilitate subsequent controller design, we construct the error signal as follows:

$$e = \begin{pmatrix} e_1 \\ e_2 \\ e_3 \end{pmatrix} = \begin{pmatrix} \theta \\ s_1 \\ s_2 \end{pmatrix} - T_e \begin{pmatrix} \theta^* \\ s_1^* \\ s_2^* \end{pmatrix}, \tag{12}$$

https://doi.org/10.1017/S0263574714001581 Published online by Cambridge University Press

where θ^* is the desired orientation of mobile robot,

$$T_e = \begin{pmatrix} 1 & 0 & 0 \\ 0 & \cos\theta_e & -\sin\theta_e \\ 0 & \sin\theta_e & \cos\theta_e \end{pmatrix},$$

and $\theta_e = \theta - \theta^*$, which can be estimated using the motion estimation technique.[9]

It can be observed in (12) that when the error $e \to 0$, one can obtain

$$\theta \to \theta^*, \quad s_1 \to s_1^*, \quad s_2 \to s_2^*. \tag{13}$$

Based on (10), (11), and (13), it is clear that the image coordinate $p_1 \to p_1^*$, $p_2 \to p_2^*$, and the orientation error $\theta_e \to 0$, that is, the current and desired images, are the same; the mobile robot reaches the desired pose.

Accordingly, the control object of the vision-based pose stabilization is to design a control law for u such that $\lim_{t\to\infty} e = 0$ and $\lim_{t\to\infty} u = 0$.

Remark 3: Based on Assumption 3, the values of p_2 and p_2^* are bounded away from zero, that is, $p_2 \neq 0$ and $p_2^* \neq 0$ for all time. From (10) and (11), we can know that s_1, s_2, s_1^*, and s_2^* are bounded. Therefore, the error signal defined in (12) is bounded and reasonable. In addition, to estimate the orientation error θ_e, at least two feature points with non-zero height parameters and not lying on the same perpendicular line with respect to the motion plane of the mobile robot are required.[9]

4. Controller Design

In this section, we will combine the dynamic surface control with backstepping and adaptive control for the electrically driven nonholonomic mobile robot described by (1)–(3) to solve the vision-based stabilization problem. The design of the control law u is proceeding step by step.

Step 1: Consider the robot kinematics (1). The error signal e defined in (12) is selected as the first dynamic surface.

Substituting (1), (8), and (9) into the time derivative of (12), the following error dynamic system can be obtained:

$$\begin{cases} \dot{e}_1 = \dfrac{r}{2L}(w_1 - w_2), \\ \dot{e}_2 = -\dfrac{r}{2L}(w_1 - w_2)e_3, \\ \dot{e}_3 = \dfrac{r}{2h}(w_1 + w_2) + \dfrac{r}{2L}(w_1 - w_2)e_2, \end{cases} \tag{14}$$

where h is the height information of the feature point P in the camera frame and is constant, that is, $h \triangleq z_c$.

To further facilitate the subsequent control design and analysis, we define $v = (v_0, \omega)^T$, where v_0, ω are the linear and angular velocities of the mobile robot respectively. The relationship between the wheel angular velocities and the velocity vector v is

$$w = \begin{pmatrix} w_1 \\ w_2 \end{pmatrix} = \begin{pmatrix} a_1 & a_2 \\ a_1 & -a_2 \end{pmatrix} v, \tag{15}$$

where $a_1 = r^{-1}$ and $a_2 = Lr^{-1}$.

Substituting (15) into (14) results in

$$\begin{cases} \dot{e}_1 = \omega, \\ \dot{e}_2 = -\omega e_3, \\ \dot{e}_3 = h^{-1}v_0 + \omega e_2. \end{cases} \tag{16}$$

https://doi.org/10.1017/S0263574714001581 Published online by Cambridge University Press

The auxiliary control law for v is chosen as

$$\begin{cases} v_{0d} = -k_1 sgn(h)\eta, \\ \omega_d = -k_2 \left(e_1 + \beta \left(e_2^2 - \eta e_3\right)\right), \end{cases} \tag{17}$$

where $\eta = e_3 + \beta e_2$, k_1, k_2 are positive constants, β is a non-zero constant, and

$$sgn(h) = \begin{cases} 1, & if\ h > 0 \\ -1 & if\ h < 0 \end{cases} \tag{18}$$

Then the virtual control law $\bar{w} = (\bar{w}_1, \bar{w}_2)^T$ is chosen as

$$\begin{aligned} \bar{w} &= \begin{pmatrix} \bar{w}_1 \\ \bar{w}_2 \end{pmatrix} \\ &= \begin{pmatrix} \hat{a}_1 & \hat{a}_2 \\ \hat{a}_1 & -\hat{a}_2 \end{pmatrix} v_d \\ &= \begin{pmatrix} a_1 - \tilde{a}_1 & a_2 - \tilde{a}_2 \\ a_1 - \tilde{a}_1 & -a_2 + \tilde{a}_2 \end{pmatrix} v_d, \end{aligned} \tag{19}$$

where $v_d = (v_{0d}, \omega_d)^T$; $\hat{a}_1$ and $\hat{a}_2$ are the estimations of a_1 and a_2 respectively; $\tilde{a}_i = a_i - \hat{a}_i$, $i = 1, 2$.

Substituting (19) into (14) results in

$$\begin{pmatrix} \dot{e}_1 \\ \dot{e}_2 \\ \dot{e}_3 \end{pmatrix} = \frac{1}{h}\left(1 - \frac{\tilde{a}_1}{a_1}\right) v_{0d} \begin{pmatrix} 0 \\ 0 \\ 1 \end{pmatrix} + \left(1 - \frac{\tilde{a}_2}{a_2}\right) \omega_d \begin{pmatrix} 1 \\ -e_3 \\ e_2 \end{pmatrix}. \tag{20}$$

The parameter update laws are given by

$$\begin{cases} \dot{\hat{a}}_1 = -\lambda_1 \mathrm{sgn}(h)\eta v_{0d}, \\ \dot{\hat{a}}_2 = -\lambda_2 \left(e_1 + \beta \left(e_2^2 - \eta e_3\right)\right) \omega_d. \end{cases} \tag{21}$$

where λ_1 and λ_2 are positive constants. Then to obtain the filtered virtual control $w_f = (w_{f1}, w_{f2})^T$, we pass $\bar{w}$ through the first-order filter,

$$\kappa_1 \dot{w}_f + w_f = \bar{w}, \quad w_f(0) = \bar{w}(0) \tag{22}$$

with a time constant $\kappa_1 > 0$.

Remark 4: Despite the height parameter h is unknown, the proposed controller (17) only depends on its sign, which can be determined according to the sign of p_2 defined in (5). In (5), y_c denotes the depth information, and we know that $y_c > 0$. So, if $p_2 > 0$, then $h > 0$; if $p_2 < 0$, then $h < 0$. In addition, p_2 can be directly computed from the image pixel coordinate using (6). Therefore, the value of $sgn(h)$ defined in (18) is known.

Step 2: Consider the robot dynamics (2). Define the second dynamic surface $S_1 = (S_{11}, S_{12})^T$ as

$$S_1 = w - w_f. \tag{23}$$

Differentiating (23) and using (2) results in

$$\begin{aligned} \dot{S}_1 &= \dot{w} - \dot{w}_f \\ &= \bar{M}^{-1}(-\bar{V} w - \bar{\tau}_d + \tau) - \dot{w}_f \\ &= \bar{M}^{-1}(\tau + \Lambda_1 \Omega_1 - \bar{\tau}_d), \end{aligned} \tag{24}$$

https://doi.org/10.1017/S0263574714001581 Published online by Cambridge University Press

where Λ_1 and Ω_1 are defined as

$$\begin{aligned}
\Lambda_1 &= \begin{pmatrix} A & B \end{pmatrix}, \quad \Omega_1 = \begin{pmatrix} C & D \end{pmatrix}^T, \\
A &= \begin{pmatrix} -(w_1 - w_2)w_2 & 0 \\ 0 & (w_1 - w_2)w_1 \end{pmatrix}, \\
B &= \begin{pmatrix} -\dot{w}_{f1} & -\dot{w}_{f2} & 0 & 0 \\ 0 & 0 & -\dot{w}_{f2} & -\dot{w}_{f1} \end{pmatrix}, \\
\dot{w}_{f1} &= \frac{\bar{w}_1 - w_{f1}}{\kappa_1}, \quad \dot{w}_{f2} = \frac{\bar{w}_2 - w_{f2}}{\kappa_1}, \\
C &= \begin{pmatrix} 0.25L^{-2}r^3 m_b d & 0.25L^{-2}r^3 m_b d \end{pmatrix}, \\
D &= \begin{pmatrix} m_1 & m_2 & m_1 & m_2 \end{pmatrix}.
\end{aligned}$$

The virtual control law $\bar{\tau} = (\bar{\tau}_1, \bar{\tau}_2)^T$ is chosen as[14]

$$\bar{\tau} = -K_1 S_1 - \hat{a}_3 \frac{\Lambda_1 \Lambda_1^T}{2\gamma_1^2} S_1, \tag{25}$$

where K_1 is the positive diagonal constant matrix; γ_1 is a positive constant; and $\hat{a}_3$ is the estimate of the unknown parameter $a_3 = \|\Omega_1\|^2$.

The parameter update law is given by

$$\dot{\hat{a}}_3 = \lambda_3 \frac{S_1^T \Lambda_1 \Lambda_1^T S_1}{2\gamma_1^2}, \tag{26}$$

where λ_3 is a positive constant. Then, $\bar{\tau}$ is passed through the following first-order filter to obtain the filtered virtual control law $\tau_f = (\tau_{f1}, \tau_{f2})^T$:

$$\kappa_2 \dot{\tau}_f + \tau_f = \bar{\tau}, \quad \tau_f(0) = \bar{\tau}(0), \tag{27}$$

where κ_2 is a positive time constant.

Step 3: Consider the actuator dynamics (3). To obtain the actual control input $u = (u_1, u_2)^T$, the third dynamic surface $S_2 = (S_{21}, S_{22})^T$ is defined as

$$S_2 = \tau - \tau_f. \tag{28}$$

Substituting (3) into the time derivative of (28) results in

$$\begin{aligned}
\dot{S}_2 &= \dot{\tau} - \dot{\tau}_f \\
&= \bar{L}_a^{-1}(u - \bar{R}_a \tau - K_e N w - u_d) - \dot{\tau}_f \\
&= \bar{L}_a^{-1}(u - \bar{R}_a \tau - K_e N w - \bar{L}_a \dot{\tau}_f - u_d) \\
&= \bar{L}_a^{-1}(u + \Lambda_2 \Omega_2 - u_d),
\end{aligned} \tag{29}$$

where Λ_2 and Ω_2 are defined as

$$\begin{aligned}
\Lambda_2 &= \begin{pmatrix} A_1 & A_2 & A_3 \end{pmatrix}, \quad \Omega_2 = \begin{pmatrix} B_1 & B_2 \end{pmatrix}^T, \\
A_1 &= \begin{pmatrix} -\tau_1 & 0 \\ 0 & -\tau_2 \end{pmatrix}, A_2 = \begin{pmatrix} -w_1 & 0 \\ 0 & -w_2 \end{pmatrix}, A_3 = \begin{pmatrix} -\dot{\tau}_{f1} & 0 \\ 0 & -\dot{\tau}_{f2} \end{pmatrix},
\end{aligned}$$

https://doi.org/10.1017/S0263574714001581 Published online by Cambridge University Press

$$B_1 = \begin{pmatrix} \frac{r_{a1}}{n_1 k_{t1}} & \frac{r_{a2}}{n_2 k_{t2}} & n_1 k_{e1} \end{pmatrix}, \quad \dot{\tau}_{f1} = \frac{\bar{\tau}_1 - \tau_{f1}}{\kappa_2},$$
$$B_2 = \begin{pmatrix} n_2 k_{e2} & \frac{l_{a1}}{n_1 k_{t1}} & \frac{l_{a2}}{n_2 k_{t2}} \end{pmatrix}, \quad \dot{\tau}_{f2} = \frac{\bar{\tau}_2 - \tau_{f2}}{\kappa_2}.$$

Then the actual control law u is chosen as

$$u = -K_2 S_2 - \hat{a}_4 \frac{\Lambda_2 \Lambda_2^T}{2\gamma_2^2} S_2, \tag{30}$$

where K_2 is the positive diagonal constant matrix; γ_2 is a positive constant; $\hat{a}_4$ is the estimate of the unknown parameter $a_4 = \|\Omega_2\|^2$, and it is updated by

$$\dot{\hat{a}}_4 = \lambda_4 \frac{S_2^T \Lambda_2 \Lambda_2^T S_2}{2\gamma_2^2} \tag{31}$$

with a positive constant λ_4.

Assumption 4: $a_i, i = 1, 2, 3, 4$ are bounded such that $0 < a_{i\min} \le a_i \le a_{i\max}$. *Remark 5*: Assumption 4 is used to facilitate the stability analysis.

In addition, to reduce the external disturbances $\bar{\tau}_d$ and u_d, robust compensators are introduced in the virtual controller $\bar{\tau}$ and the actual controller u as follows:

$$\bar{\tau} = -K_1 S_1 - \hat{a}_3 \frac{\Lambda_1 \Lambda_1^T}{2\gamma_1^2} S_1 - \varphi_1, \tag{32}$$

$$u = -K_2 S_2 - \hat{a}_4 \frac{\Lambda_2 \Lambda_2^T}{2\gamma_2^2} S_2 - \varphi_2, \tag{33}$$

where $\varphi_i = (\varphi_{i1}, \varphi_{i2})^T, \ i = 1, 2$, are robustness terms defined by[16]

$$\begin{aligned} \varphi_{ij} &= d_i \tanh\left(\frac{2k_0 d_i S_{ij}}{\varepsilon_i}\right), \\ k_0 &= 0.2785, \quad j = 1, \ 2, \end{aligned} \tag{34}$$

where $\varepsilon_i, \ i = 1, 2$, are any bounded time-varying positive scalars, i.e., $0 < |\varepsilon_i(t)| \le \varepsilon_{Mi}$ with ε_{Mi} positive constants. The robustness terms φ_i satisfy the following conditions:

$$\begin{aligned} &1. \ S_{ij}\varphi_{ij} \ge 0, \quad j = 1, \ 2, \\ &2. \ d_i \left|S_{ij}\right| - S_{ij}\varphi_{ij} \le \frac{\varepsilon_i(t)}{2}, \quad j = 1, \ 2. \end{aligned} \tag{35}$$

Remark 6: Although there are total nine unknown parameters in Ω_1 and Ω_2, the proposed controller (32) and (33) require only two tuning parameters using the simplified parameter estimation technique.[14] In addition, by introducing the first-order filters at each step of the backstepping design procedure, the proposed controller does not require the repeated differentiations of virtual controllers. This advantage of the DSC technique provides a simple design when the dynamics of the mobile robot is extended to the actuator level.

A complete structure of the proposed control scheme is shown in Fig. 2.

5. Stability Analysis

Theorem 1: Consider the electrically driven nonholonomic mobile robot described by (1)–(3) under Assumptions 1–4. The proposed controllers (19), (32), and (33) with the conditions (35) and the

https://doi.org/10.1017/S0263574714001581 Published online by Cambridge University Press

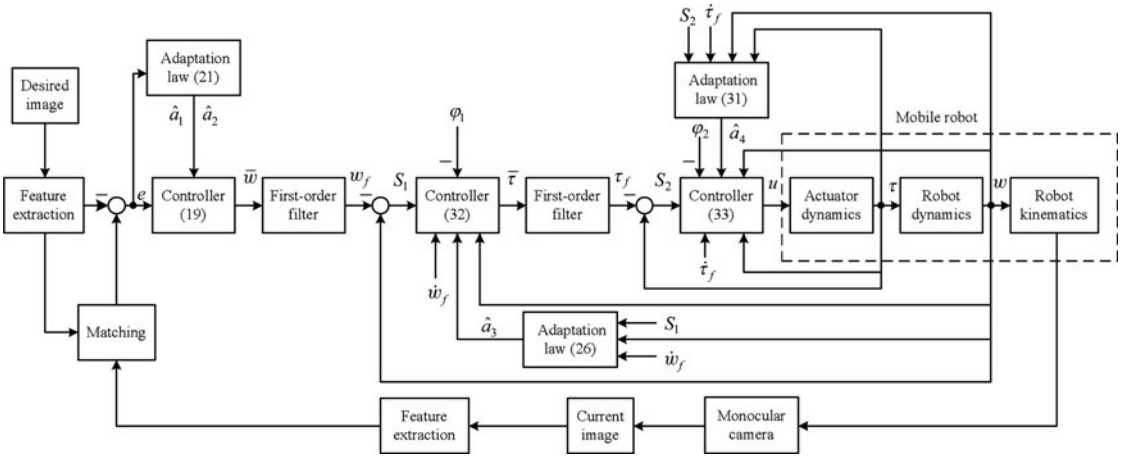

Fig. 2. Complete structure of the control scheme.

adaptation laws (21), (26), and (31) guarantee that all signals in the closed-loop system are uniformly ultimately bounded and the error systems (14), (24), and (29) can achieve asymptotic stabilization.

Proof: Define the boundary layer errors as

$$\zeta_1 = w_f - \bar{w}, \tag{36}$$

$$\zeta_2 = \tau_f - \bar{\tau}. \tag{37}$$

Taking the time derivative of (36) and (37) results in

$$\dot{\zeta}_1 = \dot{w}_f - \dot{\bar{w}} = -\frac{\zeta_1}{\kappa_1} + \Psi_1, \tag{38}$$

$$\dot{\zeta}_2 = \dot{\tau}_f - \dot{\bar{\tau}} = -\frac{\zeta_2}{\kappa_2} + \Psi_2, \tag{39}$$

where Ψ_1 and Ψ_2 are defined as

$$\Psi_1 = -\begin{pmatrix} \dot{\hat{a}}_1 v_{0d} + \hat{a}_1 \dot{v}_{0d} + \dot{\hat{a}}_2 \omega_d + \hat{a}_2 \dot{\omega}_d \\ \dot{\hat{a}}_1 v_{0d} + \hat{a}_1 \dot{v}_{0d} - \dot{\hat{a}}_2 \omega_d - \hat{a}_2 \dot{\omega}_d \end{pmatrix},$$

$$\Psi_2 = K_1 \dot{S}_1 + \frac{1}{2\gamma_1^2}(\dot{\hat{a}}_3 \Lambda_1 \Lambda_1^T S_1 + \hat{a}_3 \dot{\Lambda}_1 \Lambda_1^T S_1 + \hat{a}_3 \Lambda_1 \dot{\Lambda}_1^T S_1 + \hat{a}_3 \Lambda_1 \Lambda_1^T \dot{S}_1 + \dot{\varphi}_1).$$

Then we consider the following Lyapunov function candidate:

$$V = V_1 + V_2, \tag{40}$$

where

$$V_1 = \frac{1}{2}e_1^2 + \frac{1}{2}e_2^2 + \frac{1}{2}\eta^2 + \frac{sgn(h)}{h}\frac{\tilde{a}_1^2}{2\lambda_1 a_1} + \frac{\tilde{a}_2^2}{2\lambda_2 a_2},$$

$$V_2 = \frac{1}{2}S_1^T \bar{M} S_1 + \frac{1}{2}S_2^T \bar{L}_a S_2 + \frac{\tilde{a}_3}{2\lambda_3} + \frac{\tilde{a}_4}{2\lambda_4} + \frac{1}{2}\zeta_1^T \zeta + \frac{1}{2}\zeta_2^T \zeta_2,$$

https://doi.org/10.1017/S0263574714001581 Published online by Cambridge University Press

Herein $\eta = e_3 + \beta e_2, \tilde{a}_i = a_i - \hat{a}_i,\ i = 1,\ 2,\ 3,\ 4$ denote the estimation errors of a_i. Clearly, $V \geq 0$. Substituting (17), (20), and (21) into the time derivative of V_1 yields

$$\begin{aligned}
\dot{V}_1 &= e_1\left(1-\frac{\tilde{a}_2}{a_2}\right)\omega_d - e_2e_3\left(1-\frac{\tilde{a}_2}{a_2}\right)\omega_d + \eta\left[\frac{1}{h}\left(1-\frac{\tilde{a}_1}{a_1}\right)v_{0d} + \left(1-\frac{\tilde{a}_2}{a_2}\right)\omega_d e_2\right] \\
&\quad - \beta\eta\left(1-\frac{\tilde{a}_2}{a_2}\right)e_3\omega_d + \frac{sgn(h)}{h}\frac{\tilde{a}_1}{\lambda_1 a_1}\dot{\tilde{a}}_1 + \frac{\tilde{a}_2}{\lambda_2 a_2}\dot{\tilde{a}}_2 \\
&= \left[e_1 + \beta\left(e_2^2 - \eta e_3\right)\right]\omega_d + \frac{1}{h}\eta v_{0d} \\
&\quad - \frac{1}{h}\frac{\tilde{a}_1}{a_1}\left[\eta v_{0d} + \frac{sgn(h)}{\lambda_1}\dot{\hat{a}}_1\right] \\
&\quad - \frac{\tilde{a}_2}{a_2}\left\{\left[e_1 + \beta\left(e_2^2 - \eta e_3\right)\right]\omega_d + \frac{1}{\lambda_2}\dot{\hat{a}}_2\right\} - k_2\left[e_1 + \beta\left(e_2^2 - \eta e_3\right)\right]^2 - \frac{sgn(h)}{h}k_1\eta^2.
\end{aligned} \tag{41}$$

The time derivative of V_2 along (24), (29), (38), and (39) is given by

$$\begin{aligned}
\dot{V}_2 &= S_1^T\bar{M}S_1 + \frac{1}{2}S_1^T\dot{\bar{M}}S_1 + S_2^T\bar{L}_a\dot{S}_2 + \frac{1}{2}S_2^T\dot{\bar{L}}_aS_2 - \frac{1}{\lambda_3}\tilde{a}_3\dot{\hat{a}}_3 - \frac{1}{\lambda_4}\tilde{a}_4\dot{\hat{a}}_4 + \zeta_1^T\dot{\zeta}_1 + \zeta_2^T\dot{\zeta}_2 \\
&= S_1^T(\tau + \Lambda_1\Omega_1 - \bar{\tau}_d) + S_2^T(u + \Lambda_2\Omega_2 - u_d) - \frac{1}{\lambda_3}\tilde{a}_3\dot{\hat{a}}_3 \\
&\quad - \frac{1}{\lambda_4}\tilde{a}_4\dot{\hat{a}}_4 - \frac{1}{\kappa_1}\|\zeta_1\|^2 - \frac{1}{\kappa_2}\|\zeta_2\|^2 + \zeta_1^T\Psi_1 + \zeta_2^T\Psi_2 \\
&\leq S_1^T\bar{\tau} + \frac{(S_1^T\Lambda_1\Omega_1)(S_1^T\Lambda_1\Omega_1)^T}{2\gamma_1^2} + \frac{\gamma_1^2}{2} + S_2^Tu \\
&\quad + \frac{(S_2^T\Lambda_2\Omega_2)(S_2^T\Lambda_2\Omega_2)^T}{2\gamma_2^2} + \frac{\gamma_2^2}{2} - \frac{1}{\lambda_3}\tilde{a}_3\dot{\hat{a}}_3 - \frac{1}{\lambda_4}\tilde{a}_4\dot{\hat{a}}_4 \\
&\quad - \frac{1}{\kappa_1}\|\zeta_1\|^2 - \frac{1}{\kappa_2}\|\zeta_2\|^2 + \zeta_1^T\Psi_1 + \zeta_2^T\Psi_2 - S_1^T\bar{\tau}_d - S_2^Tu_d \\
&\leq S_1^T\bar{\tau} + \frac{a_3S_1^T\Lambda_1\Lambda_1^TS_1}{2\gamma_1^2} + S_2^Tu + \frac{a_4S_2^T\Lambda_2\Lambda_2^TS_2}{2\gamma_2^2} + \frac{\gamma_1^2}{2} \\
&\quad + \frac{\gamma_2^2}{2} - \frac{1}{\lambda_3}\tilde{a}_3\dot{\hat{a}}_3 - \frac{1}{\lambda_4}\tilde{a}_4\dot{\hat{a}}_4 - \frac{1}{\kappa_1}\|\zeta_1\|^2 - \frac{1}{\kappa_2}\|\zeta_2\|^2 \\
&\quad + \zeta_1^T\Psi_1 + \zeta_2^T\Psi_2 - S_1^T\bar{\tau}_d - S_2^Tu_d,
\end{aligned} \tag{42}$$

where the Young's inequality (i.e., $z_1z_2 \leq z_1^2/2 + z_2^2/2$) has been used.

Substituting (26), (31)–(34) into (42) and using (35) result in

$$\begin{aligned}
\dot{V}_2 &\leq -S_1^TK_1S_1 - S_2^TK_2S_2 - \frac{1}{\kappa_1}\|\zeta_1\|^2 - \frac{1}{\kappa_2}\|\zeta_2\|^2 + \tilde{a}_3\frac{S_1^T\Lambda_1\Lambda_1^TS_1}{2\gamma_1^2} - \frac{1}{\lambda_3}\tilde{a}_3\dot{\hat{a}}_3 + \tilde{a}_4\frac{S_2^T\Lambda_2\Lambda_2^TS_2}{2\gamma_2^2} \\
&\quad - \frac{1}{\lambda_4}\tilde{a}_4\dot{\hat{a}}_4 + \frac{\gamma_1^2}{2} + \frac{\gamma_2^2}{2} + \zeta_1^T\Psi_1 + \zeta_2^T\Psi_2 \\
&\quad - S_1^T\varphi_1 - S_1^T\bar{\tau}_d - S_2^T\varphi_2 - S_2^Tu_d \\
&\leq -S_1^TK_1S_1 - S_2^TK_2S_2 - \frac{1}{\kappa_1}\|\zeta_1\|^2 - \frac{1}{\kappa_2}\|\zeta_2\|^2 \\
&\quad + \frac{\gamma_1^2}{2} + \frac{\gamma_2^2}{2} + \zeta_1^T\Psi_1 + \zeta_2^T\Psi_2 + \varepsilon_1 + \varepsilon_2,
\end{aligned} \tag{43}$$

https://doi.org/10.1017/S0263574714001581 Published online by Cambridge University Press

where the fact that

$$
\begin{aligned}
-S_1^T\varphi_1 - S_1^T\bar{\tau}_d - S_2^T\varphi_2 - S_2^T u_d &= -\sum_{i=1}^{2}(S_{1i}\varphi_{1i} + S_{1i}\bar{\tau}_{di}) - \sum_{i=1}^{2}(S_{2i}\varphi_{2i} + S_{2i}u_{di}) \\
&\le -\sum_{i=1}^{2}(S_{1i}\varphi_{1i} - |S_{1i}|\,|\bar{\tau}_{di}|) - \sum_{i=1}^{2}(S_{2i}\varphi_{2i} - |S_{2i}|\,|u_{di}|) \\
&\le \sum_{i=1}^{2}(d_1|S_{1i}| - S_{1i}\varphi_{1i}) + \sum_{i=1}^{2}(d_2|S_{2i}| - S_{2i}\varphi_{2i}) \\
&\le \frac{1}{2}\varepsilon_1 + \frac{1}{2}\varepsilon_1 + \frac{1}{2}\varepsilon_2 + \frac{1}{2}\varepsilon_2 = \varepsilon_1 + \varepsilon_2
\end{aligned}
$$

has been used.

Substituting (41) and (43) into the time derivative of the Lyapunov function V defined in (40) results in

$$
\begin{aligned}
\dot{V} &\le -k_1\frac{sgn(h)}{h}\eta^2 - k_2\left[e_1 + \beta(e_2^2 - \eta e_3)\right]^2 - S_1^T K_1 S_1 - S_2^T K_2 S_2 - \frac{1}{\kappa_1}\|\zeta_1\|^2 - \frac{1}{\kappa_2}\|\zeta_2\|^2 \\
&\quad + \frac{\gamma_1^2}{2} + \frac{\gamma_2^2}{2} + \zeta_1^T\Psi_1 + \zeta_2^T\Psi_2 + \varepsilon_1 + \varepsilon_2 \\
&\le -k_1'\eta^2 - k_2\left[e_1 + \beta\left(e_2^2 - \eta e_3\right)\right]^2 - S_1^T K_1 S_1 \\
&\quad - S_2^T K_2 S_2 - \frac{1}{\kappa_1}\|\zeta_1\|^2 - \frac{1}{\kappa_2}\|\zeta_2\|^2 + \|\zeta_1\|\,\|\Psi_1\| \\
&\quad + \|\zeta_2\|\,\|\Psi_2\| + \frac{\gamma_1^2}{2} + \frac{\gamma_2^2}{2} + \varepsilon_1 + \varepsilon_2 \\
&\le -S_3^T K_3 S_3 - S_1^T K_1 S_1 - S_2^T K_2 S_2 - \frac{1}{\kappa_1}\|\zeta_1\|^2 \\
&\quad - \frac{1}{\kappa_2}\|\zeta_2\|^2 + \frac{\|\zeta_1\|^2\|\Psi_1\|^2}{2\delta_1} + \frac{\|\zeta_2\|^2\|\Psi_2\|^2}{2\delta_2} \\
&\quad + \frac{\delta_1}{2} + \frac{\delta_2}{2} + \frac{\gamma_1^2}{2} + \frac{\gamma_2^2}{2} + \varepsilon_1 + \varepsilon_2,
\end{aligned}
\tag{44}
$$

where $S_3 = [\eta, e_1 + \beta(e_2^2 - \eta e_3)]^T$, $k_1' = k_1 sgn(h) h^{-1} > 0$, δ_1 and δ_2 are positive constants, and $K_3 = \mathrm{diag}(k_1', k_2)$.

Since for any $\xi > 0$, the sets

$$
\Pi_1 := \left\{ e_1^2 + e_2^2 + \eta^2 + \frac{sgn(h)}{h}\frac{\tilde{a}_1^2}{2\lambda_1 a_1} + \frac{\tilde{a}_2^2}{2\lambda_2 a_2} + S_1^T\bar{M}S_1 + \zeta_1^T\zeta_1 \right\} \le 2\xi, \tag{45}
$$

$$
\Pi_2 := \left\{ e_1^2 + e_2^2 + \eta^2 + \frac{sgn(h)}{h}\frac{\tilde{a}_1^2}{\lambda_1 a_1} + \frac{\tilde{a}_2^2}{\lambda_2 a_2} + S_1^T\bar{M}S_1 + S_2^T\bar{L}_a S_2 + \zeta_1^T\zeta_1 + \zeta_2^T\zeta_2 + \frac{\tilde{a}_3}{\lambda_3} \right\} \le 2\xi \tag{46}
$$

are compact in R^9 and R^{14} respectively, there exist positive constants ρ_1, ρ_2 such that $\|\Psi_1\| \le \rho_1$ on Π_1 and $\|\Psi_2\| \le \rho_2$ on Π_2. Consider this fact and choose

$$
\kappa_1^{-1} = \kappa_1^* + \frac{\rho_1^2}{2\delta_1}, \quad \kappa_2^{-1} = \kappa_2^* + \frac{\rho_2^2}{2\delta_2} \tag{47}
$$

https://doi.org/10.1017/S0263574714001581 Published online by Cambridge University Press

with $\kappa_1^*,\ \kappa_2^*$ as positive constants, then we have

$$\begin{aligned}
\dot{V} &\le -S_3^T K_3 S_3 - S_1^T K_1 S_1 - S_2^T K_2 S_2 - \sum_{i=1}^{2}\left[\left(\kappa_i^* + \frac{\rho_i^2}{2\delta_i}\right)\|\zeta_i\|^2 - \frac{\|\zeta_i\|^2\,\|\Psi_i\|^2}{2\delta_i}\right] \\
&\quad + \frac{\delta_1}{2} + \frac{\delta_2}{2} + \frac{\gamma_1^2}{2} + \frac{\gamma_2^2}{2} + \varepsilon_1 + \varepsilon_2 \\
&= -S_3^T K_3 S_3 - S_1^T K_1 S_1 - S_2^T K_2 S_2 - \sum_{i=1}^{2}\left[\kappa_i^*\|\zeta_i\|^2 + \left(1 - \frac{\|\Psi_i\|^2}{\rho_i^2}\right)\frac{\rho_i^2\,\|\zeta_i\|^2}{2\delta_i}\right] + \varepsilon \\
&= -S_1^T K_1 S_1 - S_2^T K_2 S_2 - S_3^T K_3 S_3 - S_4^T K_4 S_4 - S_5^T K_5 S_5 + \varepsilon \\
&= -\psi^T K \psi + \varepsilon \\
&\le -\varsigma_{\min}(K)\,\|\psi\|^2 + \varepsilon,
\end{aligned} \tag{48}$$

where

$$S_4 = \left(\|\zeta_1\|, \sqrt{1 - \frac{\|\Psi_1\|^2}{\rho_1^2}}\,\|\zeta_1\|\right)^T, \quad K_4 = \operatorname{diag}\left(\kappa_1^*, \frac{\rho_1^2}{2\delta_1}\right),$$

$$S_5 = \left(\|\zeta_2\|, \sqrt{1 - \frac{\|\Psi_2\|^2}{\rho_2^2}}\,\|\zeta_2\|\right)^T, \quad K_5 = \operatorname{diag}\left(\kappa_2^*, \frac{\rho_2^2}{2\delta_2}\right),$$

$$\varepsilon = \frac{\delta_1}{2} + \frac{\delta_2}{2} + \frac{\gamma_1^2}{2} + \frac{\gamma_2^2}{2} + \varepsilon_1 + \varepsilon_2,$$

$$\psi^T = \left(S_1^T, S_2^T, S_3^T, S_4^T, S_5^T\right),\ K = \operatorname{diag}(K_1, K_2, K_3, K_4, K_5),$$

and $\varsigma_{\min}(K)$ is the minimum eigenvalue of matrix K. Thus, $\dot{v}$ is strictly negative outside the following compact set Ξ_ψ:

$$\Xi_\psi = \left\{\psi(t)\,\middle|\, 0 \le \|\psi\| \le \sqrt{\frac{\varepsilon}{\varsigma_{\min}(K)}}\right\}. \tag{49}$$

Under the conclusion that $\hat{a}_i,\ i = 1, 2, 3, 4$ are uniformly ultimately bounded (it is easy to prove that $\hat{a}_i \in [a_{i\,\min}, a_{i\,\max}]$ under Assumption 4, which is omitted here), we can conclude that $\|\psi\|$ decreased whenever ψ is outside the compact set Ξ_ψ, and hence $\|\psi\|$ is uniformly ultimately bounded. Therefore, all signals in the closed-loop system are uniformly ultimately bounded. Besides, by adjusting the control gains K, the error systems (14), (24), and (29) can achieve asymptotic stabilization.

6. Simulation Results

In this section, simulation results are provided to show the validity of the developed controller for the vision-based pose stabilization of the electrically driven nonholonomic mobile robot. The initial pose of the mobile robot is chosen as $(-1.5,\ -5,\ \pi/9)^T$ and the desired one is $(0, 0, 0)^T$. The simulated data are obtained by generating a virtual landmark comprising three feature points not lying on the same vertical plane. The feature points of the landmark are projected to the image plane using a virtual camera: the focal length of the camera being $f = 6$ mm and the size of the virtual images is 640×480 pixels. The parameters with appropriate units of robot and actuators are chosen as follows:

$$r = 0.15,\ L = 0.75, \quad d = 0.3, \quad m_b = 30, \quad m_w = 1,$$
$$I_c = 15.625, \quad I_w = 0.005, \quad I_m = 0.0025,$$

https://doi.org/10.1017/S0263574714001581 Published online by Cambridge University Press

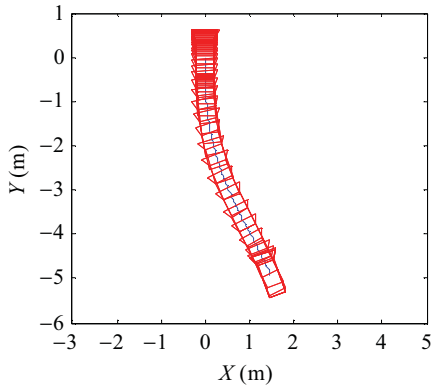

Fig. 3. Robot trajectory on the $X - Y$ plane.

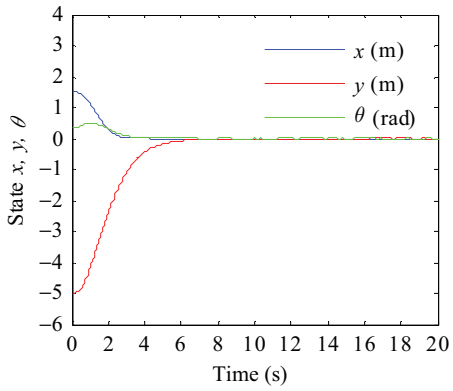

Fig. 4. State variables of robot during motion.

$$R_a = \text{diag}(1.5, 1.5), \quad L_a = \text{diag}(0.227, 0.227),$$
$$K_e = \text{diag}(0.01, 0.01), \quad K_T = \text{diag}(0.283, 0.283),$$
$$N = \text{diag}(15, 15).$$

The control gains and other parameters are chosen as

$$k_1 = 0.15, \quad k_2 = 1.8, \quad \beta = 0.001,$$
$$K_1 = \text{diag}(3.1, 3.1), \quad K_2 = \text{diag}(4.1, 8.1),$$
$$\lambda_1 = 0.045, \quad \lambda_2 = 25.5, \quad \lambda_3 = 0.01, \quad \lambda_4 = 0.1,$$
$$\gamma_1 = 7.1, \quad \gamma_2 = 8.1, \quad \kappa_1 = \kappa_2 = 0.1.$$

The initial values of $\hat{a}_1$, $\hat{a}_2$, $\hat{a}_3$, and $\hat{a}_4$ are chosen as $\hat{a}_1(0) = 0.1$, $\hat{a}_2(0) = 0.5$, $\hat{a}_3(0) = 0.1$, and $\hat{a}_4(0) = 0.1$ respectively. The disturbances are chosen to be white noises distributed uniformly with amplitude of 0.04.

The simulation results are shown in Figs. 3–10. Fig. 3 shows the upper view of the robot motion in the $X - Y$ plane. Although all exact values of the parameters of the robot and the actuators are not known *a priori* and there are external disturbances in the robot and actuator dynamics, the mobile robot is successfully driven to the desired pose with a quite small error. The corresponding behavior of the state of robot is depicted in Fig. 4. All the state variables are convergent to their desired values. The bounded control input u by using the proposed controller is shown in Fig. 5. We can note that the actuator voltages asymptotically tend to zero except the external disturbances. Besides, the error signal e, the wheel angular velocity error S_1, and the wheel torque error S_2 can be corrected quickly by the controller depicted in Figs. 6–8. In Fig. 6, we can see that the system error e tends to zero

https://doi.org/10.1017/S0263574714001581 Published online by Cambridge University Press

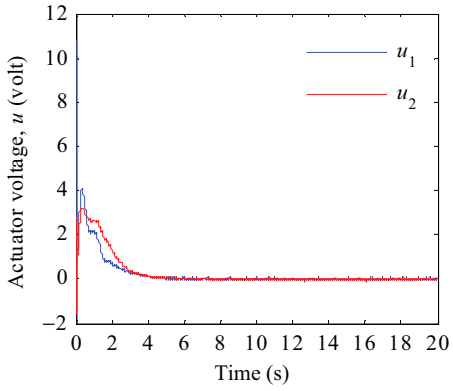

Fig. 5. Control input, $u = [u_1, u_2]^T$.

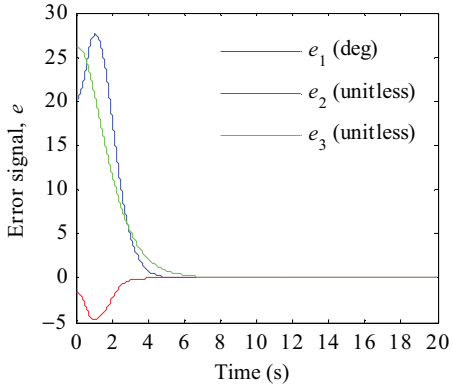

Fig. 6. Error signal, $e = [e_1, e_2, e_3]^T$.

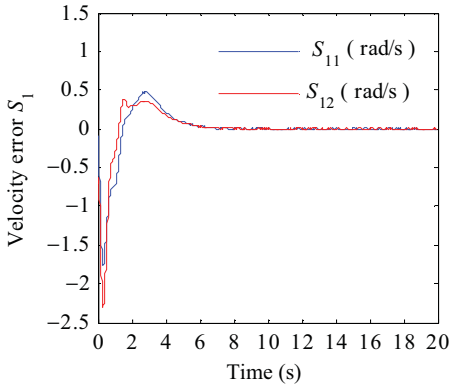

Fig. 7. Wheel angular velocity error, $S_1 = [S_{11}, S_{12}]^T$.

(about 6.5 s), which implies that the current image gradually converges to the desired one. From Figs. 7 and 8, we can see that the actual wheel angular velocity and wheel torque asymptotically reach their desired ones in about 6.0 s and 5.0 s respectively. The responses of the estimated unknown parameters are given in Figs. 9 and 10. It is shown that all the signals are bounded, and that $\hat{a}_1$ and $\hat{a}_2$ approach to their actual values $a_1 = r^{-1} = 6.67$ and $a_1 = r^{-1}L = 5$ respectively. We can also see that the estimated parameters reach their desired values in about 3.0 s.

To illustrate the performance of the controller with image noise, a random noise with a standard deviation of 0.3 pixels is added to feature points. The results are shown in Figs. 11–16. We can observe that the control objective can still be achieved with quite a small error in spite of the existence of image noise. Fig. 11 shows the image trajectory of three feature points. The presence of the image noise is

https://doi.org/10.1017/S0263574714001581 Published online by Cambridge University Press

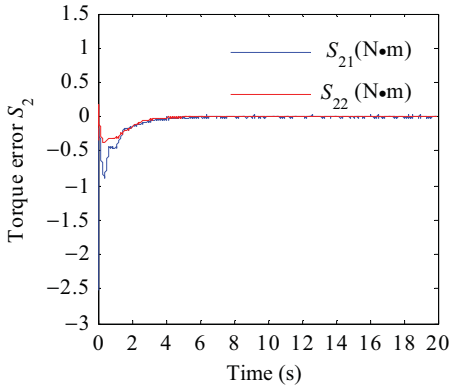

Fig. 8. Wheel torque error $S_2 = [S_{21}, S_{22}]^T$.

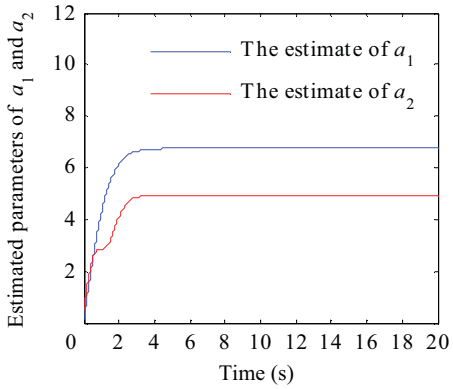

Fig. 9. Responses of $\hat{a}_1$ and $\hat{a}_2$.

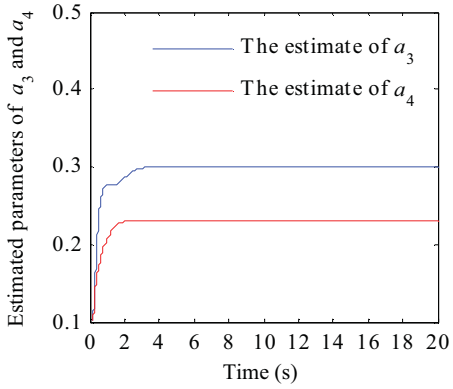

Fig. 10. Responses of $\hat{a}_3$ and $\hat{a}_4$.

clear and we can see that the current image gradually tends to the desired image, which implies that the robot is driven to its desired pose asymptotically. In Fig. 12, we can see the exponential behavior of the robot state. In spite of image noise, the control input u depicted in Fig. 13 is also bounded and finally tends to zero. Figs. 14–16 show the error signal e, the wheel angular velocity error S_1, and the wheel torque error S_2 respectively, all of which converge to zero. All of the simulation results verify the effectiveness of the proposed controller.

https://doi.org/10.1017/S0263574714001581 Published online by Cambridge University Press

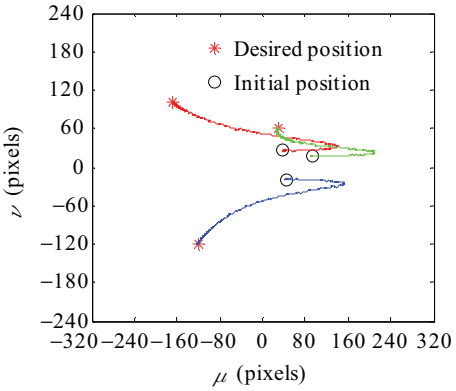

Fig. 11. Trajectory of feature points in the image.

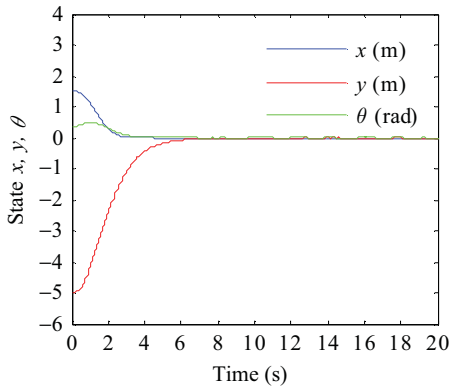

Fig. 12. State variables of robot during motion.

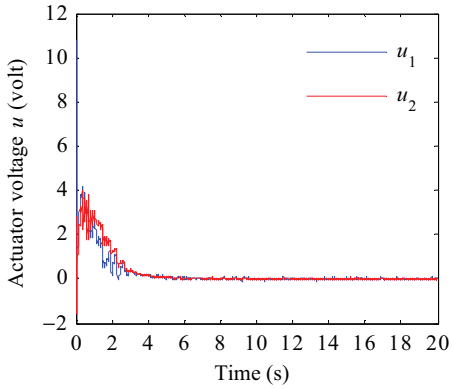

Fig. 13. Control input, $u = [u_1, u_2]^T$.

7. Conclusions

Following are the conclusions:

1. A robust adaptive dynamic surface controller has been presented to perform the vision-based pose stabilization of a nonholonomic mobile robot, including actuator dynamics with parametric uncertainties and disturbances.
2. By incorporating the DSC method with backstepping, the repeated differentiations of virtual controllers can be avoided, and the parametric uncertainties and disturbances can be compensated by the robust adaptive technique. In addition, the number of tuning parameters has been reduced by using the simplified parameter estimation technique.

https://doi.org/10.1017/S0263574714001581 Published online by Cambridge University Press

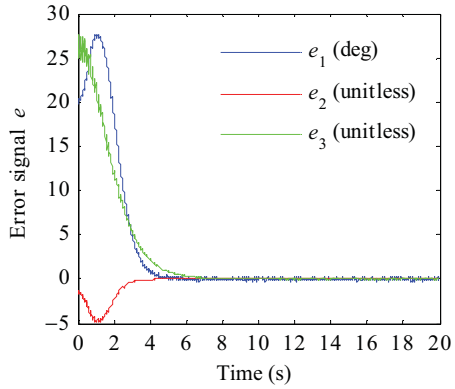

Fig. 14. Error signal, $e = [e_1, e_2, e_3]^T$.

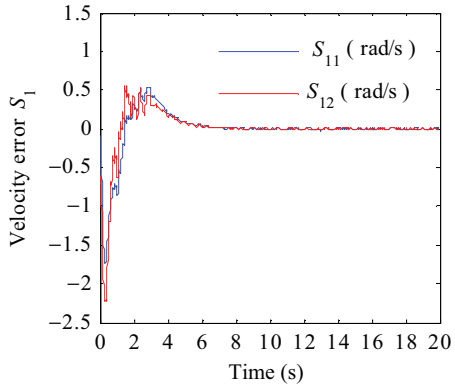

Fig. 15. Wheel angular velocity error, $S_1 = [S_{11}, S_{12}]^T$.

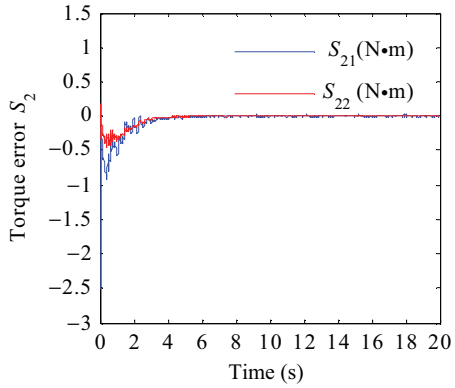

Fig. 16. Wheel torque error, $S_2 = [S_{21}, S_{22}]^T$.

3. The proposed controller can drive the robot to its desired pose in spite of lack of depth information and does not require any *a priori* knowledge of robot and actuator's parameters. From the Lyapunov stability theory, it is shown that all signals in the close-loop system are uniformly ultimately bounded. Simulation results have been provided to demonstrate the performance of the proposed controller.

https://doi.org/10.1017/S0263574714001581 Published online by Cambridge University Press

Acknowledgements
This work is supported by the National Natural Science Foundation of China (No. 61105089), State Key Laboratory of Robotics and System (No.SKLRS-2013-ZD-03) and Open Foundation of the State Key Laboratory of Fluid Power Transmission and Control (No.GZKF-201212).

References

1. G. L. Mariottini, D. Prattichizzo and G. Oriolo, "Epipole-based visual servoing for nonholonomic mobile robots," **In**: *Proceedings of the IEEE International Conference on Robotic Automation*, New Orleans, LA, United States (Apr. 26–May 1, 2004) pp. 497–503.
2. G. L. Mariottini, G. Oriolo and D. Prattichizzo, "Image-based visual servoing for nonholonomic mobile robots using epipolar geometry," *IEEE Trans. Robot.* **23**(1), 87–100 (Feb. 2007).
3. H. M. Becerra and C. Sagues, "A sliding-mode-control law for mobile robots based on epipolar visual servoing from three views," *IEEE Trans. Robot.* **27**(1), 175–183 (Feb. 2011).
4. Y. Fang, W. E. Dixon, D. M. Dawson and P. Chawda, "Homography-based visual servo regulation of mobile robots," *IEEE Trans. Syst. Man Cybern. B* **35**(5), 1041–1050 (Oct. 2005).
5. G. Lopez-Nicolas, C. Sagues and J. J. Guerrero, "Homography-based visual control of nonholonomic vehicles," **In**: *Proceedings of the IEEE International Conference on Robotic Automation*, Roma, Italy (Apr. 10–14, 2007) pp. 1703–1708.
6. G. Lopez-Nicolas, J. J. Guerrero and C. Sagues, "Visual control of vehicles using two-view geometry," *Mechatronics* **20**(2), 315–325 (Mar. 2010).
7. H. M. Becerra and C. Sagues, "A novel 1D trifocal tensor-based control for differential-drive robots," **In**: *Proceedings* of the *IEEE International Conference on Robotic Automation*, Kobe, Japan (May 12–17, 2009) pp. 1104–1109.
8. G. Lopez-Nicolas, J. J. Guerrero and C. Sagues, "Visual control through the trifocal tensor for nonholonomic robots," *Robot. Autom. Syst.* **58**(2), 216–226 (Feb. 2010).
9. X. Zhang, Y. Fang and X. Liu, "Motion-estimation-based visual servoing of nonholonomic mobile robots," *IEEE Trans. Robot.* **27**(6), 1167–1175 (Dec. 2011).
10. C. Wang, "Visual servoing feedback-based robust regulation of nonholonomic wheeled mobile robots," **In**: *Proceedings of the IEEE International Conference on Robotic Automation*, Shanghai, China (May 9–13, 2011) pp. 6174–6179.
11. Z. L. Wang and Y. H. Liu, "Visual regulation of a nonholonomic wheeled mobile robot with two points using Lyapunov functions," **In**: *Proceedings* of the *IEEE International Conference on Mechatronics and Automation*, Xi'an, China (Aug. 4–7, 2010) pp. 1603–1608.
12. F. Yang and C. Wang, "Adaptive stabilization for uncertain nonholonomic mobile robots based on visual servoing feedback," *Acta Autom. Sinica* **37**(7), 857–864 (July 2011).
13. Z. Li, S. S. Ge, M. Adams and W. S. Wijesoma, "Adaptive robust output-feedback motion/force control of electrically driven nonholonomic mobile manipulators," *IEEE Trans. Control Syst. Technol.***16**(16), 1308–1315 (Nov. 2008).
14. B. S. Park, S. J. Yoo, J. B. Park and Y. H. Choi, "A simple adaptive control approach for trajectory tracking of electrically driven nonholonomic mobile robots," *IEEE Trans. Control Syst. Technol.* **18**(5), 1199–1206 (Sep. 2010).
15. K. Shojaei, A. M. Shahri, A. Tarakameh and B. Tabibian, "Adaptive trajectory tracking control of a differential drive wheeled mobile robot," *Robotica* **29**(3) 391–402 (May 2011).
16. Z. Hou, A. Zou, L. Cheng and M. Tan, "Adaptive control of an electrically driven nonholonomic mobile robot via backstepping and fuzzy approach," *IEEE Trans. Control Syst. Technol.* **17**(4) 803–815 (July 2009).
17. D. Swaroop, J. K. Hedrick, P. P. Yip and J. C. Gerdes, "Dynamic surface control for a class of nonlinear systems," *IEEE Trans. Autom. Control* **45**(10), 1893–1899 (Oct. 2000).
18. T. Fukao, H. Nakagawa and N. Adachi, "Adaptive control of a nonholonomic mobile robot," *IEEE Trans. Robot. Autom.* **16**(5), 609–615 (Oct. 2000).